

## A three-dimensional solution for the orbit of the asteroidal satellite of 22 Kalliope

F. Marchis,<sup>a,\*</sup> P. Descamps,<sup>b</sup> D. Hestroffer,<sup>b</sup> J. Berthier,<sup>b</sup> F. Vachier,<sup>b</sup> A. Boccaletti,<sup>c</sup>  
I. de Pater,<sup>d</sup> and D. Gavel<sup>e</sup>

<sup>a</sup> Astronomy Department, University of California, 601 Campbell Hall, Berkeley, CA 94720-3411, USA

<sup>b</sup> Institut de mécanique céleste et de calcul des éphémérides, UMR-CNRS 8028, Observatoire de Paris, 77, avenue Denfert-Rochereau, F-75014 Paris, France

<sup>c</sup> GPS—CalTech, 1200 E. California Blvd, M/S 150-21, Pasadena, CA 91125, USA

<sup>d</sup> Astronomy Department, University of California, Berkeley, CA 94720-3411, USA

<sup>e</sup> Lawrence Livermore National Laboratory/IGPP, 7000 East Avenue, Livermore, CA 94551, USA

Received 21 March 2002; revised 30 May 2003

### Abstract

We carried out new observations of the binary asteroid 22 Kalliope (S2/2001) with the Shane 3-m telescope of the Lick observatory in October and November 2001. With a FWHM (full width at half maximum) of  $0''.2$ , Kalliope (apparent size of about  $0''.15$ ) was not resolved but it was possible to separate the secondary from its primary whose apparent separation was of the order of  $0''.7$  with a magnitude difference of  $3.22 \pm 0.20$ . As each set of observations spanned a few days of time, they are well distributed along the secondary's orbit, enabling us to accurately estimate its orbit.

The satellite orbits 22 Kalliope in a prograde manner with respect to Kalliope's rotational spin (which is in a retrograde sense relative to its orbit around the Sun), on a highly inclined ( $i = 19.8 \pm 2.0$  with respect to the equator of 22 Kalliope) and moderately eccentric orbit ( $e = 0.07 \pm 0.02$ ) with an orbital period of  $3.58 \pm 0.08$  days. The semi-major axis is  $1020 \pm 40$  km. Using Kalliope's diameter as determined from IRAS data, the asteroid's bulk density is about  $2.03 \pm 0.16 \text{ g cm}^{-3}$ , suggestive of a highly porous body with a porosity of 70% considering that the grain density of its meteoritic analog is of  $\sim 7.4 \text{ g cm}^{-3}$ . This suggests a rubble pile, rather than solid, body. The measured nodal precession rate of the secondary's orbit seems to be much higher than expected from Kalliope's oblateness, assuming a homogeneous body (constant density). This suggests that Kalliope may be 60% more elongated or 35% larger than presently believed or/and that its internal structure is highly inhomogeneous with a denser outer shell.

© 2003 Elsevier Inc. All rights reserved.

**Keywords:** Asteroids; Asteroids, composition; Infrared observations; Interiors; Orbits

### 1. Introduction

Since the first asteroidal satellite discovery during the Galileo spacecraft's 1993 fly-by of Ida's moonlet, Dactyl (Chapman et al., 1995), over twenty moons have been found to orbit other small bodies in our Solar System. Nine of them are located in the main asteroid belt, and seven of them in the Kuiper belt (in addition to the Pluto–Charon system). The asteroidal moon discovery rate has dramatically increased over the past years with the advent of Adaptive Optics (AO) on ground-based telescopes. This technique provides high contrast images with a resolution close to the diffraction limit

of the telescope, which enables one to measure orbits of faint asteroidal satellites by collecting relative astrometric observations of the system. Large surveys with 3–10 m-class telescopes equipped with AO are performed (Close et al., 2000).

Observable parameters, such as the mass ratio between the components and their separation should be related to the way binary asteroid systems were formed. Thus, knowledge of these parameters for a significant sample of binaries should provide insights on the collisional history of the asteroid belt. Unfortunately among the asteroidal satellites discovered so far, there is no orbit that is known precisely enough to characterize the satellite's origin.

As a rule, by lack of sufficient data regarding asteroid satellite orbits, the orbits are usually assumed to be roughly

\* Corresponding author.

E-mail address: [fmarchis@astron.berkeley.edu](mailto:fmarchis@astron.berkeley.edu) (F. Marchis).

equatorial and circular. By measuring the separation between the components and their orbital period, the mass of the system can be inferred from Kepler's third law. A measurement of the relative brightness of the components serves to determine the individual masses. If the size of the body is known, its density can be inferred. Hence, even with the simple assumption of a circular orbit in the equatorial plane, the major physical characteristics of the asteroidal system can be determined. Yet a full description of the orbit in terms of the classical orbital parameters could bring useful further constraints regarding the internal structure of the central body.

The main goal of our study is to describe the orbit of the moonlet of 22 Kalliope (S2/2001). The binary character of this system was recently reported by (Merline et al., 2001) on H-band direct imaging obtained on September 2.6 UT, 2001 with the 3.6-m Canada–France–Hawaii telescope (+ PUEO AO system) on Mauna Kea. A few days earlier, Margot and Brown (2001) had also detected Kalliope's moonlet on AO H-band images obtained on August 29.6 and 31.6 UT, 2001 with the 10-m W. M. Keck II telescope on Mauna Kea (Margot and Brown, 2001). The projected separation between the primary and secondary was then estimated to be about  $0''.5$  (1000 km) at a position angle of  $180^\circ$ .

Our observations span a few consecutive days at two distinct periods well separated in time. Thus we can unambiguously determine all the orbital parameters and detect the secular advances of the apsidal and nodal lines due primarily to perturbations from the non-spherical shape of Kalliope.

In Section 2 we present the data collected with the two telescopes. Sections 3 and 4 summarize the astrometric method and the orbital elements measured. Constraints on the composition and internal structure of the primary are derived in Sections 5, 6, and 7. Finally (Section 8) we discuss a possible origin of this binary system.

## 2. Observations

The asteroid Kalliope had an apparent visible magnitude of  $11.0 \pm 0.3$  in October and November 2001, so it was directly observable using AO systems. Since the sensitivity limit of existing AO systems is around 14th magnitude, an excellent wavefront correction was expected.

In October 2001, we used the Shane 3-m telescope of the Lick Observatory with its AO system and the IRCAL camera developed by UC-Berkeley (Lloyd et al., 2000; Gavel et al., 2000). The camera is equipped with a PICNIC HgCdTe  $256 \times 256$  pixel detector, sensitive at 1–2.5  $\mu\text{m}$  and with a pixel size of  $0''.0765$ . Excellent observations were obtained on UT October 3, 4, and 6 (see Table 2). The first night revealed the companion in H-band (1.656  $\mu\text{m}$ ), somewhat better in K-band (2.195  $\mu\text{m}$ ) and quite marginal in J-band (1.238  $\mu\text{m}$ ). We therefore focused our program on the K-band observations with an individual integration time of 4 seconds. Object and sky frames were obtained by moving the target to 5 different positions on the detector. The

resulting image, with a total integration time of 1 minute, is composed of 15 shift-added frames. From images of a nearby star with a similar magnitude, we estimate the angular resolution (FWHM) at  $0''.157 \pm 0.004$ , and the Strehl Ratio (Ratio of observed to theoretical peak intensity) at 40–55%. This resolution is not high enough to resolve the main asteroid whose predicted angular size was  $0''.15$ , but the high signal-to-noise on the AO data enabled the detection of its companion at an angular distance of  $0''.545 \pm 0.077$ ,  $3.22 \pm 0.20$  magnitude fainter than the primary. Figure 1 shows an image taken at the Lick Observatory in the Ks band.

On 2 and 3 November 2001 (UT), observations were performed at the 3-m Shane telescope at Lick observatory, and also with the Palomar AO system (PALAO) at the Palomar 5-m telescope. Its camera, PHARO, built by the Cornell University Astronomy Department Infrared Group is a  $1024 \times 1024$  Rockwell HAWAII HgCdTe array detector (Hayward et al., 2001), sensitive also between 1–2.5  $\mu\text{m}$  and with a pixel size of  $0''.025$ . J, H, and K band data were taken on November, 1st and 2nd, 2001 using the same technique as described for the Lick data. The total integration time was  $\sim 54.5$  s and the data have an angular resolution of  $0''.097$ ,  $0''.084$ , and  $0''.094$ , respectively, at J, H, and K band (estimated on a Point Spread Function or PSF star). On these dates, the angular size of the main asteroid was  $0''.17$ . The main asteroid should therefore be slightly resolved, but we did not manage to recover its shape using a basic PSF fitting or a deconvolution process because of the time variation in the AO correction. The moonlet companion was clearly detected and well separated from the primary, allowing to accurately estimate its position relative to the primary. Figure 2 shows an image taken at the Palomar Observatory in the Ks band.

## 3. Astrometry

The CCD positions of Kalliope and its satellite are measured by centroiding with a two-dimensional Moffat–Gauss profile, especially suited to AO images (Descamps et al., 2002). The background is modeled by an inclined quadratic surface due to the strong luminosity gradient in the vicinity of Kalliope.

As there was no reference star in the small field of view, it is not possible to determine the astrometric parameters of the frames. Thus we use the theoretical ones to transform the CCD ( $x, y$ ) coordinates into celestial coordinates (see Table 1). In order to quantify the uncertainties introduced by this assumption, we carried out an astrometric calibration of the system using two images of the central part of the Trapezium cluster centered on  $\theta^1$  Ori in the Orion nebula. These images contain about 10 known stars (McCaughrean and Stauffer, 1994), which were used as reference stars to calculate the scale and orientation factors with a classical plate constants model. The astrometric parameters obtained

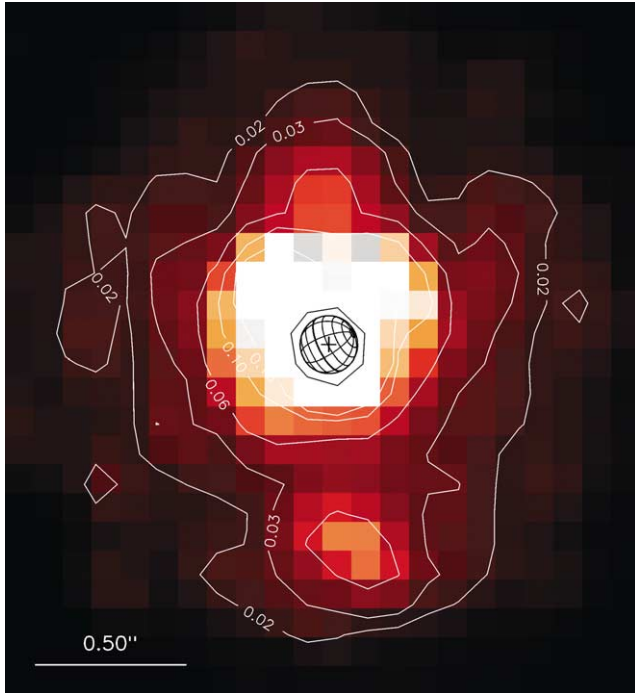


Fig. 1. Image of Kalliope with its moonlet, taken at the Lick Observatory on October, 04 at 13:18:46.5 UTC in the Ks band ( $2.15 \pm 0.32 \mu\text{m}$ ). The FWHM is  $0''.17$  and the apparent size of Kalliope is  $0''.15$ . North is up and East is right.

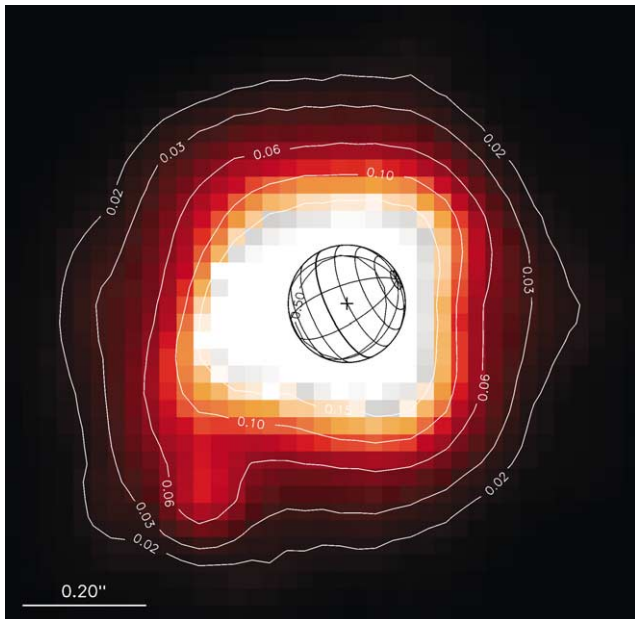


Fig. 2. Image of Kalliope with its moonlet, taken at the Palomar Observatory on 2001 November, 03 at 07:15:36 UTC in the Ks band. The FWHM is  $0''.13$  and the apparent size of Kalliope is  $0''.17$ . North is up and East is right.

are presented in Table 1. Based upon a comparison of these parameters with the theoretical ones, we trust our astrometry at a level of a few milli-arcseconds using the theoretical plate constants (Berthier and Marchis, in preparation).

Table 1

Astrometric parameters of AO system + IRCAL camera

	X scale (mas px <sup>-1</sup> )	Y scale (mas px <sup>-1</sup> )	Orientation (deg)
Image 1	$74.8 \pm 0.1$	$76.9 \pm 0.1$	$-0.04 \pm 0.01$
Image 2	$75.1 \pm 0.6$	$77.8 \pm 0.5$	$-0.23 \pm 0.01$
Theoretical	76.5	76.5	0.00

Note. Theoretical and observed astrometric parameters of the system performed on two H-band images of the central part of the Trapezium cluster centered on  $\theta^1$  Ori.

Table 2

Observations and astrometric results for 22 Kalliope and its secondary

Mid-exposure time (UTC)	X (mas)	Y (mas)	Flux ratio	$R_e$ (km)
2001 October 03				
13:12:01.5	$+125.0 \pm 22.7$	$+442.7 \pm 25.3$	14.7	24
13:24:07.0	$+142.7 \pm 11.8$	$+431.5 \pm 13.2$	21.9	18
2001 October 04				
09:47:31.5	$+160.1 \pm 10.1$	$-456.9 \pm 11.4$	23.1	19
10:56:23.5	$+154.7 \pm 8.5$	$-503.2 \pm 9.5$	24.2	19
12:54:55.5	$+62.9 \pm 10.5$	$-527.6 \pm 9.2$	15.5	23
13:18:46.5	$+61.9 \pm 9.5$	$-526.9 \pm 16.9$	15.7	24
2001 October 06				
10:09:23.5	$-101.3 \pm 13.3$	$+610.6 \pm 22.2$	20.6	19
10:38:26.0	$-92.2 \pm 8.5$	$+625.2 \pm 11.5$	21.2	20
12:50:44.5	$-71.2 \pm 14.0$	$+666.8 \pm 14.7$	20.7	21
2001 November 02				
07:23:22.00	$+145.9 \pm 1.5$	$-685.0 \pm 1.4$	17.3	21
07:30:25.00	$+144.9 \pm 4.3$	$-688.8 \pm 3.5$	20.1	20
11:33:26.50	$+75.6 \pm 2.9$	$-770.5 \pm 3.2$	18.6	20
11:40:52.00	$+75.8 \pm 2.9$	$-771.9 \pm 2.7$	20.2	20
2001 November 03				
07:15:36.00	$-195.2 \pm 3.2$	$-259.8 \pm 4.5$	18.6	21
07:19:01.00	$-174.7 \pm 4.3$	$-244.7 \pm 5.4$	17.9	21

Satellite positions are relative to Kalliope in the sense satellite minus Kalliope.

The cartesian and polar coordinates of the secondary relative to Kalliope in the tangential sky-plane collected for this analysis are listed in Table 2. The flux ratio between Kalliope and its satellite is also quoted. Although data were also acquired on October 5, it was not possible to separate the two objects, in part caused by a degraded seeing (FWHM  $\sim 0''.4$ ). On the other hand, we know that the satellite was actually near its periastron making separation of the two components particularly difficult.

#### 4. The apparent orbit

The orbital elements we determined are the semi-major axis  $a$ , eccentricity  $e$ , inclination  $i$  with respect to the equatorial plane of Kalliope, the longitude of the ascending node  $\Omega$  with respect to a common arbitrary direction (taken as the intersection of the equatorial plane of 22 Kalliope with the line of sight in October 2001), and the argument of perias-

tron  $\omega$  which determines the direction of the pericenter with respect to the equatorial plane of Kalliope.

Given the fact that our data are grouped over two well-separated periods, we made the choice to deal, at this stage, with the problem of the orbit determination in a geometric way rather than in a classical dynamic way. This, indeed, is justified since aspect changes of the Earth and the asteroid due to their motion through space can be considered as nearly constant during each run. Similarly, perturbations due to Kalliope's oblateness and by other massive bodies—especially the giant planets and the Sun—may be neglected as well. Such effects are noticeable only after a couple of days. In other words, the orbit can be considered as a snapshot in time, defined as the Keplerian orbit that would be followed if the perturbing forces were instantaneously turned off. Finally, in doing this, we avoid assumptions on plausible initial conditions. The only constraints imposed on fitting the orbit are Kepler's first two laws. The consistency of the orbit solution for each of the observing runs should confirm whether or not the dynamics of the system is controlled in a common and simple way. If not, the orbit solution may yield some valuable information on the state of rotation of Kalliope in terms of pole position or precession of its spin axis. Our model was fitted to the data using a weighted least-squares method.

For one apparent (i.e., projected onto the plane-of-sky view) observed orbit there are two Keplerian solutions with the same shape, one of which is prograde and the other is retrograde, but with an asymmetric spatial orientation. The ambiguity may be resolved from at least two observing epochs since there will be only one common solution.

As far as the November 2001 data are concerned, only three observations were obtained. In this case, the fitting process converges only if at least two parameters of the orbit are fixed. This is why we did not re-fit the orbital shape parameters  $a$  and  $e$ , but used those derived from the October observations. We can then determine the orbit's orientation in space. Table 3 lists the orbital elements for the October and November data and their  $1\sigma$  formal error as derived from the

Table 3  
Orbital elements of the Kalliope's satellite for each observing run

Element	October 2001 orbit	November 2001 orbit
Period (days)	$3.58 \pm 0.08$	$3.56 \pm 0.07$
Semi-major axis (arcsec)	$0.638 \pm 0.012$	$0.759^b$
Semi-major axis (km)	$1020 \pm 40$	$1020^b$
Argument of the pericenter (deg)	$190 \pm 60$	$347 \pm 7$
Argument of the node (deg) <sup>c</sup>	$15.0 \pm 1.5$	$8.0 \pm 0.5$
Eccentricity	$0.07 \pm 0.02$	$0.07^b$
Inclination (deg)	$18.9 \pm 2.5$	$19.5 \pm 0.6$
$\sigma_0^a$ (mas)	23	7

<sup>a</sup> Standard deviation on the polar radius for a given position angle.

<sup>b</sup> Value fixed during the fit.

<sup>c</sup> With respect to a common arbitrary direction taken as the intersection of the equatorial plane of 22 Kalliope with the plane of sight of October 2001.

diagonal elements of the covariance matrix. The symmetric solution is not reproduced here. The final adjusted trajectories are shown in Fig. 3. The ascending node  $\Omega$ , the line of nodes, the pericenter and the sense of the orbital motion are reported as well. The root mean square errors (RMS) on the whole set of data in October is  $\sim 23$  mas while it is only  $\sim 7$  mas in November where the data were acquired mainly with the Palomar 5-m telescope. After analyzing the data in the orbital plane, we were able to fit Kepler's equations, providing the mean motion. Resulting orbital periods are quoted in Table 3 as well.

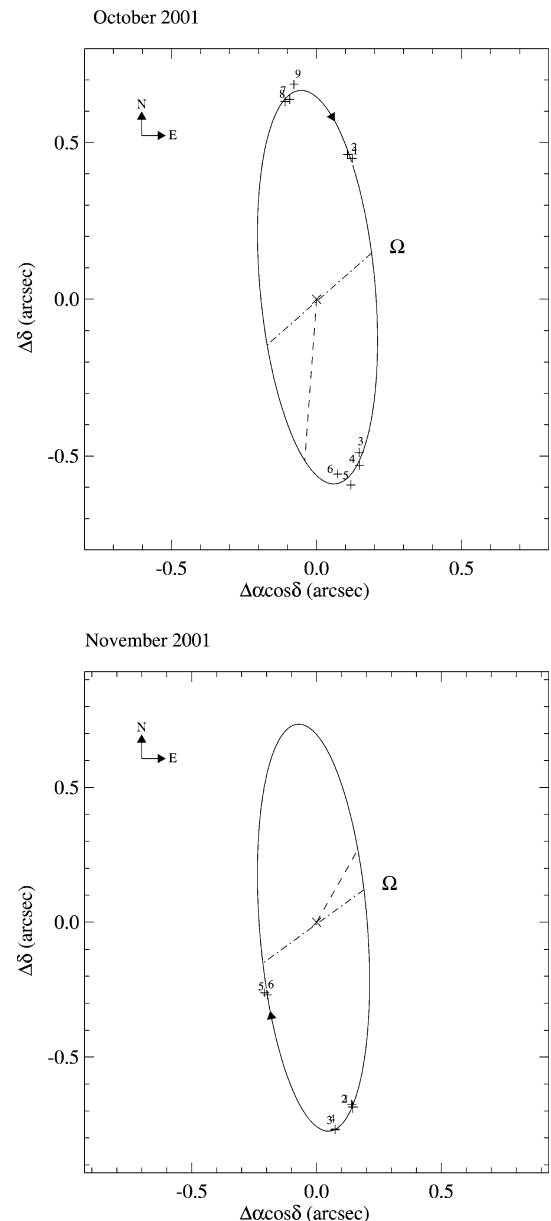


Fig. 3. Apparent orbit of the companion of 22 Kalliope on October and November 2001. Locus of the pericenter is reported by the dashed line while the nodal line is the dash-dot line. Observations are quoted with their formal errors in both coordinates.

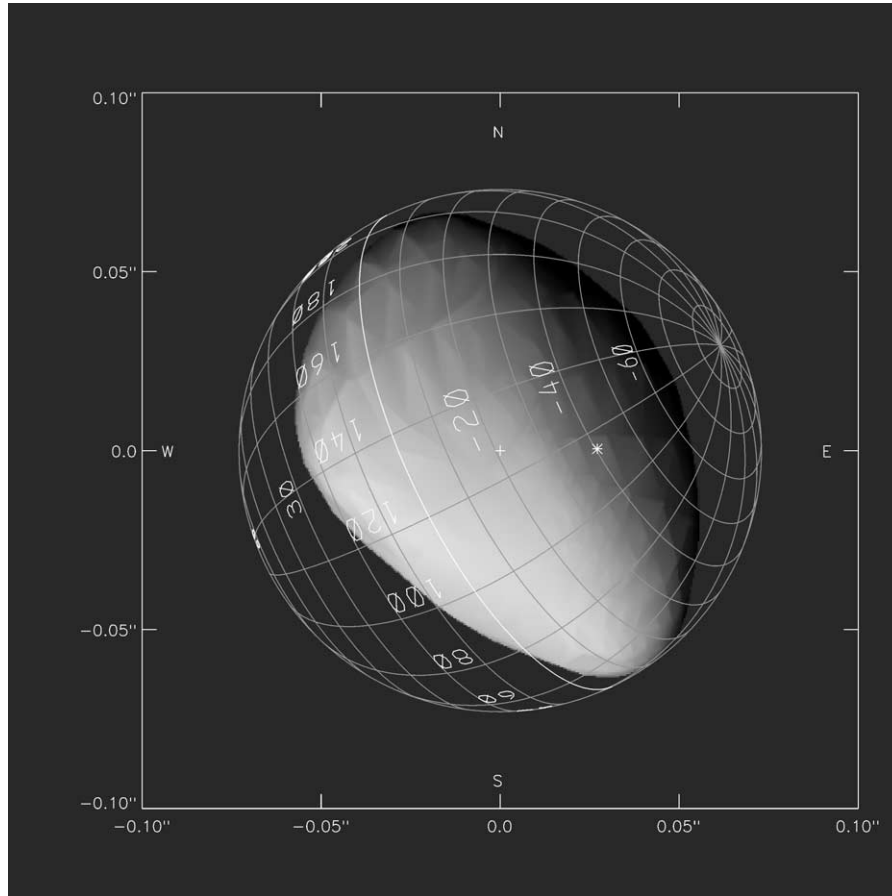


Fig. 4. Aspect of 22 Kalliope on 04 October 2001 at 13:18:46.5 UTC. The asteroid is represented by a 2036 polygons shape model with a grid step of 5 degrees (courtesy of M. Kaasalainen). Shading of the object is computed from a Minnaert scattering law with a limb darkening parameter of 0.55. The cross marks the Sub-solar point (SSP) position. The Sub-Earth point (SEP) is located at the asterisks.

In order to determine the inclination of the orbital plane with respect to Kalliope's rotational equator, and the sense of the orbital motion with respect to the primary spin, we need to know Kalliope's pole position without any ambiguity. Pole and shape solutions have been derived by (Kaasalainen et al., 2002), the latest and best solution is given in terms of ecliptic latitude and longitude in J2000,  $\lambda_0 = 20^\circ.3$  and  $\beta_0 = -22^\circ.9$  (M. Kaasalainen, private communication). Moreover, we used their shape solution as obtained from photometric data to determine the theoretical shift of the observed center of Kalliope with respect to the center of mass. With a phase angle of about  $20^\circ.0$ , this effect may reach 7 mas at most, which is near the level of accuracy of our astrometric measurements. We did not take this effect into account in our astrometric reduction. With the pole solution as given above, the apparent size and aspect of 22 Kalliope on the dates of the observation corresponding to Figs. 1 and 2 are shown in Figs. 4 and 5. Apparently, the companion orbits 22 Kalliope in the same sense as Kalliope is spinning. Since the rotation of Kalliope is retrograde, the motion of the satellite around Kalliope is also retrograde; i.e., the angular motion of the satellite's revolution around Kalliope is in a sense opposite to that of Kalliope's revolution around the Sun. Such

retrograde orbits appear to be more stable against solar perturbations than prograde orbits, where such perturbations can quite easily disrupt an orbit of a satellite that is only weakly gravitationally bound (Hamilton and Krivov, 1997; Chauvineau and Mignard, 1990).

## 5. Physical parameters of 22 Kalliope and its satellite

We used the set of orbital parameters to derive the mass of Kalliope from Kepler's third law:

$$a^3 n^2 = G(M_K + M_S)$$

where  $G = 6.67259 \times 10^{-11} \text{ m}^3 \text{ kg}^{-1} \text{ s}^{-2}$  is the universal gravitational constant,  $a$  the major semiaxis previously determined and  $n = 100.7 \pm 0.7^\circ \text{ day}^{-1}$  the mean motion of the satellite. Brightness ratios between both bodies and corresponding equivalent radius of the secondary are given in Table 2. The large scatter in this radius may suggest that the secondary is elongated rather than spheroidal, as expected from tidal distortions (Leone et al., 1984), but may come from the quality of the AO correction as well. Finally we derive a mean equivalent radius ( $R_s$ ) of  $19 \pm 3 \text{ km}$  for the

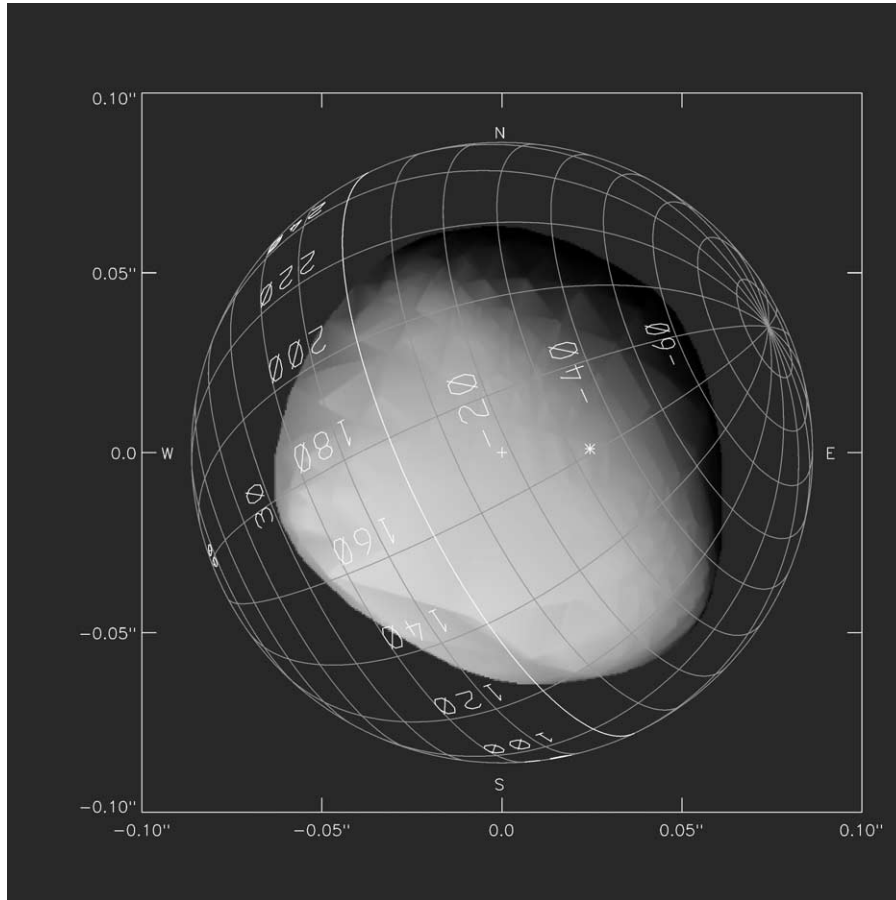


Fig. 5. Aspect of 22 Kalliope on 03 November 2001 at 07:15:36 UTC.

satellite. If we assume that the satellite and Kalliope formed upon disruption of the primary by an impact, they are made up of the same material. If we assume the satellite to have the same bulk density as Kalliope itself, we derive a mass ratio  $q = M_S/M_K$  of 0.009. Thus  $M_K \simeq (6.30 \pm 0.50) \times 10^{18}$  kg. Assuming Kalliope's radius is  $90.50 \pm 2.3$  km, as derived from IRAS data (Tedesco et al., 2002), we get a bulk density of  $2.03 \pm 0.16$  g cm $^{-3}$ . This is much lower than the density of a typical M-type meteorite, the meteoritic analog of an M-type asteroid with which 22 Kalliope has been classified.

## 6. Secular perturbations of the Kalliope's satellite orbit

Owing to the small separation between Kalliope and its satellite, the orbital dynamics reduces to the classical two-body problem, and is therefore dominated by the harmonics of the gravitational potential. Under such circumstances, the effect of Kalliope's shape on the satellite's orbit can be approximated by the  $J_2$  ( $= -C_{20}$ ) and  $C_{22}$  terms in the gravitational potential.<sup>1</sup> Moreover, because Kalliope rotates much faster around its axis than the satellite orbits the asteroid (ro-

tation period of Kalliope is 4.15 h), the secular effect of the equatorial ellipticity on the gravitational potential ( $C_{22}$  term) tends to average to zero. This leaves the zero order terms as the most significant gravitational effects on the satellite's orbit. This, in turn, is equivalent to the satellite being subject to the gravitational field of an oblate spheroid. To first order, these gravitational terms induce secular motions in the node and periastron of the satellite orbit. Comparison between numerical computations and simple analytic results for oblate spheroids show good agreement if the satellite orbit is sufficiently far away from the asteroid, if it is not too close to synchronous orbit, or if the satellite is in a retrograde orbit (Scheeres, 1994). The secular variations expressed in terms of the orbital elements then become:

$$\frac{d\omega}{dt} = \frac{3}{4} \frac{nr_e^2}{a^2(1-e^2)^2} (1 - 5\cos^2 i) C_{20},$$

$$\frac{d\Omega}{dt} = \frac{3}{2} \frac{nr_e^2}{a^2(1-e^2)^2} \cos i C_{20},$$

where  $r_e$  is a scaling radius, e.g., the equatorial radius of Kalliope (IRAS radius). We implicitly assume a principal axis coordinate frame. We specify this frame such that  $C_{20} \leq 0$ , so that the principal moments of inertia (normalized by the body mass) are ordered as  $I_X \leq I_Y \leq I_Z$  with principal axis  $X$ ,  $Y$ , and  $Z$ . The gravity coefficients can then

<sup>1</sup> It can be shown that neither the  $C_{30}$  nor the  $C_{40}$  terms have large contributions here.

be derived from the principal moments of inertia of the body:

$$J_2 = -C_{20} = -\frac{1}{2r_e^2}(I_X + I_Y - 2I_Z).$$

Taking the orbital elements derived here and the ellipsoidal figure given in the literature,  $a/b = 1.32$ ,  $b/c = 1.2$ , together with the IRAS radius (which gives the following major semi-axis:  $a = 115.71$  km,  $b = 87.67$  km,  $c = 73.06$  km), one finds, assuming a constant density,  $J_2 = 0.127$ . With the topographic shape solution of (Kaasalainen et al., 2002) we derive quite consistent results from a numerical integration over the volume of the body assuming a constant density with  $J_2 = 0.124$ .

Thus if we are able to measure the advances of the pericenter and the node between the two periods of observation, we must expect the following inclination-dependent ratio:

$$\frac{\dot{\omega}}{\dot{\Omega}} = \frac{1}{2} \left( \frac{1 - 5 \cos^2 i}{\cos i} \right).$$

Since we derived an inclination of  $19.8^\circ$ , the ratio is then equal to  $-1.82$ . With the theoretical value of  $J_2$  previously computed, we can expect a nodal rate of  $-0.13^\circ \text{ day}^{-1}$  and an apsidal rate of  $0.25^\circ \text{ day}^{-1}$ . Since our orbit determination gives an inaccurate and moderate eccentricity, the dynamical effect of the gravitational potential of 22 Kalliope is better detected from the retrograde motion of the nodal line. The latter is quite well determined due the high inclination of the orbital plane over the equatorial plane of 22 Kalliope. Conversely the position of the pericenter is poorly determined during the October run, which implies a higher uncertainty that prevents any reliable determination of the apsidal advance between the two periods. During the 30 days that separates the two observing runs, we have measured a nodal line advance of  $-7 \pm 3^\circ$  which gives an observed nodal rate of  $-24^\circ \text{ day}^{-1}$  from which we can infer an observed value of  $J_2$  of  $0.20 \pm 0.07$ . This value appears to be higher than the  $J_2$  expected from Kalliope's shape, although the lower limit of the observed value is marginally consistent with the theoretical number of 0.127.

Taking the numbers ( $J_2(\text{obs}) = 0.20$  and  $J_2(\text{theor}) = 0.127$ ) at face value, the difference can be explained by invoking a 35% higher equatorial radius or a 60% more elongated shape of 22 Kalliope. The reported IRAS uncertainty of 2.5% on the radius may be optimistic for elongated bodies (Tanga et al., 2003), and cannot account for the observed difference. Concerning the shape, the topographic solution is trustworthy and gives similar global results as the ellipsoidal solution.

At last, another possible explanation may lie in a non-uniform mass distribution inside 22 Kalliope as shown in the next section from a simple analytical model of the internal structure.

## 7. Internal structure of Kalliope: a model for the density distribution

The relatively low bulk density found above let us suggest that Kalliope has a significant porosity. If we assume the asteroid is made exclusively of iron meteoritic type material with a density of  $7.4 \text{ g cm}^{-3}$ , we find a macroporosity of 70%; but even with less dense material ( $3\text{--}5 \text{ g cm}^{-3}$ ) the porosity ranges from 33% to 60%. Considering that Kalliope (and possibly its satellite) is the outcome of a catastrophic or sub-catastrophic impact, it could be a shattered or a rubble pile body of large macroporosity and weak cohesion. The porosity would hence be related to the large-scale voids and features inside the body (Richardson et al., 2003, and references therein).

Britt and Consolmagno (2001) proposed a model to describe the structure of such bodies. Large irregular pieces (and larger voids) are probably located deep inside the asteroid, while smaller particles have accreted later onto the body, and are therefore found closer to the surface, with the finest material (formed by continuous meteorite bombardment) restricted to the surface regolith zone. The large interior voids are preserved from gravitational infilling by the effect of friction on the smaller size fractions.

Such a formation model with a density distribution much higher as we progress toward the external surface of the body may be empirically translated in a closed form by a simple density power law with two parameters written in a spherical coordinates  $(r, \theta, \phi)$  system with respect to the center of mass:

$$\rho(r, \theta, \phi) = \rho_s \left( \frac{r}{r_a(\theta, \phi)} \right)^n,$$

$r_a(\theta, \phi)$  is the topographic spherical representation of Kalliope's shape. It is in general unknown, except for a few objects from radar data or spacecraft flybys. With such a model,  $\rho_s$  may be interpreted as the grain density present on the surface. The exponent  $n$  is linked to the macroporosity present inside the object. Realistic behavior of the density impose only positive values of the exponent. A uniform density is obtained with  $n = 0$ . With such a model, the mass of Kalliope reads:

$$\begin{aligned} M_K &= \int_V \rho(r, \theta, \phi) dV \\ &= \int_V \rho_s \left( \frac{r}{r_a(\theta, \phi)} \right)^n r^2 \cos \phi dr d\theta d\phi, \\ M_K &= \frac{3\rho_s V}{n+3} = \rho_b V. \end{aligned}$$

Where  $\rho_b$  is the bulk density and  $V$  the volume of Kalliope. We can then relate the bulk density to the surface density by the simple following relation:

$$\rho_b = \frac{3}{n+3} \rho_s.$$

Finally we can express the bulk porosity  $p$  as a function of the exponent  $n$ :

$$p = 1 - \frac{\rho_b}{\rho_s} = \frac{n}{n+3}.$$

In spite of its simplicity, this model may be applied to predict global effects of mass distribution and macroporosity. Values of the exponent, smaller than unity could characterize fractured asteroids whose macroporosity may reach at most 25% (Britt et al., 2002). Beyond, the macroporosity may be the trace of a rubble pile structure. Indeed from potential terrestrial analogs and models of the breakup/reassembly process, it was predicted that rubble pile asteroids porosities must be in the range 30–75%.

In the same way we can also express the zonal harmonic  $J_2^{(n)}$  as a function of  $n$  and its value assuming a constant density  $J_2^{(0)}$  by

$$J_2^{(n)} = \frac{5}{3} \left( \frac{n+3}{n+5} \right) J_2^{(0)}.$$

With such a model we predict that the effect on the gravitational field becomes sensitive only for values of  $n$  greater than 2 or 3, hence for rubble-pile asteroids and this enhancement may reach at most 66%. In other words, measuring the  $J_2^{(0)}$  is a way to access the macroporosity of an object without any assumption on the composition of the aggregate material.

As an example, if we apply the model to the S-type asteroid 433 Eros for which a comprehensive determination of the gravity field by the NEAR-Shoemaker spacecraft in February 2000 was made (Miller et al., 2002), we get  $n = 0.65$  from an estimated macroporosity of 18% (Britt et al., 2002). It gives a  $J_2$  ratio  $J_2^{(n)}/J_2^{(0)} = 1.07$ . As the true gravity field measured by NEAR is very close to the one determined from the shape model assuming constant density (with a ratio of 0.993), we can say that our simple model is a good approximation within a few percent.

The  $J_2^{(n)}$  value derived above requires a macroporosity exponent of 8 corresponding to a macroporosity of 71%. If we consider that an M type asteroid is made of a material without microporosity, we get a grain density of  $7.0 \text{ g cm}^{-3}$  which is fairly consistent with the analog iron meteorite grain density of  $7.4 \text{ g cm}^{-3}$ .

## 8. Possible origin of the binary system

We identified three possible scenarios of formation described in (Weidenschilling et al., 1989): cratering ejecta, disruptive capture and rotational fission. Kalliope's satellite was most likely formed from cratering ejecta produced by a sub-catastrophic impact, as pointed out by Merline et al. (2003), because the orbital motion is prograde, the mass ratio is of the order of 0.01, the primary is rotating in less than 6 h and the primary is significantly non-spherical. However

one then needs to explain how to produce ejecta from a sub-catastrophic impact and a very porous primary, which seems difficult to obtain. A catastrophic collision could also lead to a satellite in orbit around a primary from a disruptive capture, as suggested for Dactyl in orbit around 243 Ida (Belton et al., 1996), but this may be more unlikely for Kalliope because it is not part of a dynamical family. Another slightly different scenario would be that the companion comes from ejecta produced by rotational fission even though the spin rate may not be fast enough. In this scenario, an off-center impact delivers enough angular momentum to an asteroid that its spin rate exceeds the breakup point for a strengthless body. The asteroid sheds mass, and a companion forms close to the primary. But this would preferably produce a same-size binary, so one needs to explain the small size of the satellite and its high inclination.

## 9. Conclusion

Direct AO observations of a binary asteroid by means of high resolution imaging with large optical instruments coupled with a long-term astrometric monitoring program allows one to determine the apparent orbit of the secondary and its precession, which yields crucial information about the physical properties and the internal density structure of the asteroid.

We have reported here the first observations of orbital precession of the binary asteroid 22 Kalliope. We have computed the mass of Kalliope from the orbit of its moon; with the known size of the primary, we derived a density of  $2.0 \pm 0.16 \text{ g cm}^{-3}$  for Kalliope, a M-type asteroid, which suggests a highly porous, or rubble pile object. From a comparison of the gravitational moment  $J_2$  as derived from Kalliope's shape, with that derived from the orbital precession of its moonlet, we suggest that 22 Kalliope has a non-uniform mass distribution, with a denser outer shell than interior. Furthermore, the determination of the secondary's orbit yield information on its formation scenario. We identified two possible, but imperfect, scenarios. Most likely, the satellite could have been formed from cratering ejecta after a sub-catastrophic impact. In this case, one has to identify how such an impact can produce ejecta and a very porous primary. We can also suppose that the companion is an effect of a rotational fission after an off-center impact, but this will preferably produce a same size binary and it is difficult to explain the high inclination.

A follow-up with Adaptive Optics on ground-based telescopes of binary asteroidal systems including a study of the companion orbits, as described here, gives crucial information about the internal structure of the asteroids that may only be inferred otherwise from space mission flybys.

## Acknowledgments

This work has been supported in part by the National Science Foundation Science and Technology Center for Adap-

tive Optics, managed by the University of California at Santa Cruz under cooperative agreement No. AST-9876783. The observers thank the Lick support team for their assistance during these observations.

## References

- Berthier, J., Marchis, F., in preparation, Astrometric calibration of the ADO-NIS/SHARPII+/Nimos 3 device in use at ESO 3.60 m telescope.
- Belton, M.J.S., Mueller, E.A., D'Amario, L.A., Byrnes, D.V., Klaasen, K.P., Synnot, S., Breneman, H., Johnson, T.V., Thomas, P.C., Veverka, J., Harch, P.A., Davies, D., Merline, W.J., Chapman, C.R., Davis, D., Denk, T., Neukum, G., Petit, J.-M., Greenberg, R., Storrs, A., Zellner, B., 1996. The discovery and orbit of 1993 (243)1 Dactyl. *Icarus* 120, 185–199.
- Britt, D.T., Consolmagno, G.J., 2001. Modeling the structure of high porosity asteroids. *Icarus* 152, 134–139.
- Britt, D.T., Yeomans, D., Housen, K., Consolmagno, G.J., 2002. Asteroid density, porosity, and structure. In: Bottke, W., Cellino, A., Paolichi, P., Binzel, R. (Eds.), *Asteroids III*. Univ. of Arizona Press, Tucson, pp. 485–500.
- Chapman, C.R., Veverka, J., Thomas, P.C., Klaasen, K., Belton, M.J.S., Harch, A., McEwen, A., Johnson, T.V., Helfenstein, P., Davies, M.E., Merline, W.J., Denk, T., 1995. Discovery and physical properties of Dactyl a satellite of asteroid 243 Ida. *Nature* 374, 783.
- Chauvineau, B., Mignard, F., 1990. Dynamics of binary asteroids. I—Hill's case. *Icarus* 83, 360–381.
- Close, L.M., Merline, W.J., Dumas, C., Chapman, C.R., Roddier, F.J., Ménard, F., Slater, D., Duvert, G., Shelton, J., Morgan, T.H., 2000. Search for asteroidal satellites using adaptive optics. In: Wizinowich, P.L. (Ed.), *Adaptive Optical Systems Technology*. In: Proc. SPIE, Vol. 4007, pp. 796–802.
- Descamps, P., Marchis, F., Berthier, J., Prangé, R., Fusco, T., Le Guyader, C., 2002. First ground-based astrometric observations of Puck. *C. R. Physique* 3, 121–128.
- Gavel, D.T., Olivier, S.S., Baumann, B.J., Max, C.E., Macintosh, B.A., 2000. Progress with the Lick adaptive optics system. In: Proc. SPIE, Vol. 4007, pp. 63–70.
- Hamilton, D.P., Krivov, A.V., 1997. Dynamics of distant moons of asteroids. *Icarus* 128, 241–249.
- Hayward, T.L., Brandl, B., Pirger, B., Blacken, C., Gull, G.E., Schoenwald, J., Houck, J.R., 2001. PHARO: A near-infrared camera for the Palomar adaptive optics system. *Publ. Astron. Soc. Pacific* 113 (779), 105–118.
- Kaasalainen, M., Torppa, J., Piironen, J., 2002. Models of twenty asteroids form photometric data. *Icarus* 159, 369–395.
- Leone, G., Paolicchi, P., Farinella, P., Zappala, V., 1984. Equilibrium models of binary asteroids. *Astron. Astrophys.* 140, 265–272.
- Lloyd, J.P., Liu, M.C., Macintosh, B.A., Severson, S.A., Deich, W.T., Graham, J.R., 2000. IRCAL: the infrared camera for adaptive optics at Lick Observatory. In: Proc. SPIE, Vol. 4008, pp. 814–821.
- McCaughrean, M.J., Stauffer, J.R., 1994. High resolution near-infrared imaging of the Trapezium: a stellar census. *Astron. J.* 108, 1382–1397.
- Merline, W.J., Ménard, F., Close, L., Dumas, C., Chapman, C.R., Slater, D.C., 2001. *IAU Circ.* 7703.
- Margot, J.-L., Brown, M.E., 2001. *IAU Circ.* 7703.
- Merline, W.J., Weidenschilling, S.J., Durda, D.D., Margot, J.-L., Pravec, P., Storrs, A.D., 2003. Asteroids DO have satellites. In: Bottke, W., Cellino, A., Paolichi, P., Binzel, R. (Eds.), *Asteroids III*. Univ. of Arizona Press, Tucson, pp. 289–312.
- Miller, J.K., Konopliv, A.S., Antreasian, P.G., Bordi, J.J., Chesley, S., Helfrich, C.E., Owen, W.M., Wang, T.C., Williams, B.G., Yeomans, D.K., Scheeres, D.J., 2002. Determination of shape, gravity and rotational state of Asteroid 433 Eros. *Icarus* 155, 3–17.
- Richardson, D.C., Leinhardt, Z.M., Melosh, H.J., Bottke Jr., W.F., Asphaug, E., 2003. Gravitational aggregates: evidence and evolution. In: Bottke, W., Cellino, A., Paolichi, P., Binzel, R. (Eds.), *Asteroids III*. Univ. of Arizona Press, Tucson, pp. 485–500.
- Scheeres, D.J., 1994. Dynamics about uniformly rotating triaxial ellipsoids: applications to asteroids. *Icarus* 110, 225–238.
- Tanga, P., Hestroffer, D., Cellino, A., Lattanzi, M., Di Martino, M., Zappalà, V., 2003. Asteroid observations with the Hubble Space Telescope. II. Duplicity search and size measurements for 6 asteroids. *Astron. Astrophys.* 401, 733–741.
- Tedesco, E.F., Noah, P.V., Noah, M., Price, S.D., 2002. *Astron. J.* 123, 1056.
- Weidenschilling, S.J., Paolicchi, P., Zappalà, V., 1989. Do asteroids have satellites? In: Binzel, R., Gehrels, T., Matthews, M. (Eds.), *Asteroids II*. Univ. of Arizona Press, Tucson, pp. 643–658.